Springer

Acta Mechanica Sinica

CrossMark click for updates

•RESEARCH PAPER•

Acta Mech. Sin., Vol. 38, 322062 (2022)
https://doi.org/10.1007/s10409-022-22062-4

Effect of rib height on turbulent flow and heat transfer of kerosene in rectangular duct

Xian Li[1,2], Fengquan Zhong[1,2*], and Yunfei Xing[1]

[1] *State Key Laboratory of High Temperature Gas Dynamics, Institute of Mechanics, Chinese Academy of Sciences, Beijing 100190, China;*
[2] *School of Engineering Science, University of Chinese Academy of Sciences, Beijing 100049, China*

Received March 1, 2022; accepted March 29, 2022; published online May 10, 2022

The coupling effects of rib heights and fluid properties on turbulent convective heat transfer of kerosene flow through the rectangular duct on the ribbed bottom wall are studied numerically in this paper. The numerical simulation is based on the ten components surrogate model of kerosene and the Reynolds average method combined with the re-normalized group (RNG) k-ε turbulence model. The turbulent vortex structures and heat transfer characteristics of kerosene flowing over rectangular ribs of different heights are obtained. The results show that three dimensional vortices are generated by the ribs, and the vortices alter local flow significantly, leading to both enhanced and reduced convective heat transfer at different locations near the ribs. In addition, it is found that with the increase of rib height, the average Nusselt number and the wall friction factor on the ribbed wall also increase. For the present study, the maximum heat transfer enhancement rate of kerosene flow is 72.16%, and the ratio of rib-to-duct height is 0.75.

Rib height, Kerosene, Heat transfer enhancement, Turbulent flow

Citation: X. Li, F. Zhong, and Y. Xing, Effect of rib height on turbulent flow and heat transfer of kerosene in rectangular duct, Acta Mech. Sin. **38**, 322062 (2022), https://doi.org/10.1007/s10409-022-22062-4

1. Introduction

The rib is a mini-structure that can efficiently improve heat transfer performance for active cooling ducts. When the coolant flows through the channel with ribs on the wall, the fluid is disturbed, which promotes turbulence and forms a strong vortex structure as well as strengthens heat transfer [1-3]. Rib cooling has been widely applied to numerous engineering applications, such as nuclear reactors [4], gas turbine cooling [5], and solar thermal systems [6], etc.

The geometry and arrangement of rib affect turbulent flow structure significantly and cause various heat transfer distributions. Especially, rib shapes, rib sizes (including the rib height and width, etc.), and rib-to-rib distances notably influence the heat transfer performance. Kamali and Binesh [7] developed computer codes which can well simulate the distributions of frictional resistance and heat transfer caused by air flowing in a 50 mm×50 mm square duct with ribs of various shapes. Promvonge and Thianpong [8] conducted experiments to study the heat transfer and wall friction characteristics of airflow in rectangular ducts with ribs of different shapes such as a triangular, wedge, and rectangular. With the infrared thermography technique, SriHarsha et al. [9] obtained the heat transfer distribution of air channel flow on the ribbed wall with different rib heights. The results of this experiment present that as the rib height increases, the Nusselt number caused by ribs increases gradually, and the corresponding pressure loss also increases greatly. Kim et al. [10] used the Reynolds average method and optimization technique to obtain the attack angles of ribs for the best thermal performances in rectangular ducts with the cross-section of 40 mm×40 mm. Through the experimental methods, Skullong et al. [11] investigated the effects of the size and arrangement of ribs on airflow through the rectangular channel used in the solar air heater. Sharma et al. [12] carried out experiments to study the flow field and heat transfer in

*Corresponding author. E-mail address: fzhong@imech.ac.cn (Fengquan Zhong)
Executive Editor: Zhixiang Xiao

rectangular ducts with ribs of different shapes, displayed vortices by a particle image velocimetry (PIV) and measured temperatures by liquid crystal thermography (LCT). Oleiwi and Al-Turaihi [13] researched numerically and experimentally the effects of rib heights on air-water two-phase flowing through vertical ducts.

As shown above, the previous pieces of literature have focused on the heat transfer and flow field of fluids with simple physical properties, such as water or air, whose physical properties remain unchanged with temperature. However, there are very few studies [14,15] on the flow structures of hydrocarbon fuels in ribbed cooling ducts. It is worth noticing that hydrocarbon fuels have been widely used as the coolant of active thermal protection in aerospace engine applications [16,17]. At present, extensive researches about the heat transfer performances of the hydrocarbon fuel flowing through the smooth straight cooling duct have been conducted [18-20]. To the author's knowledge, the influence of rib structure on the flow vortex structures and heat transfer properties of hydrocarbon fuels have not been well studied yet. In order to explore the cooling properties of the rib in kerosene flow, the small rectangular duct is numerically studied in this paper. The coupling effect of rib heights and kerosene properties on the heat transfer characteristics and flow structures is particularly concerned.

2. Configuration and boundary conditions

The turbulent convective heat transfer performances of kerosene flowing in rectangular ducts with ribs of different heights are investigated numerically in the current study. Figure 1 presents the geometrical configuration of the rectangular cooling duct. The rectangular duct has the length of 130 mm, the width of 5 mm, and the height of 2 mm, respectively. As shown in the figure, there are ten rectangular ribs aligned on the bottom wall of the duct along the flow direction, and they are periodically distributed along the spanwise direction. The spacing (s) from the duct entrance to the first rib is 60.5 mm. The length (e) and the width (w) of ribs are 3 mm and 1 mm, and the position (p) between every adjacent two ribs is 5 mm. The height of rib (h) is set to vary from 0.25 to 1.5 mm with a distance of 0.25 mm.

Figure 2 shows the schematic of boundary conditions for a computational domain. As shown in the figure, the constant heat flux loaded on the top and bottom walls of the duct is 500 kW/m^2, which is a typical heat flow value of aero-engines in Ref. [21]. The periodic boundary condition is applied on both sides of the computational domain. The cooling medium is kerosene and the inlet mass flow rate is 12 g/s. Besides, the inlet pressure and temperature of kerosene are set to 4 MPa and 300 K, respectively. The outflow boundary is used for an outlet. The physical parameters of kerosene, including thermodynamic and transport properties, are obtained by the ten components surrogate model established in our previous research [20]. Therefore, the kerosene flowing in the rectangular duct is fully turbulent for the present study, because the Reynolds number at the duct inlet is 3700, which is greater than the critical value of 2300 for turbulent duct flow. And the gravity effect is ignored since the ratio of Grashof number to the square of Reynolds number is very small and less than 10^{-4}.

The Reynolds number in this paper is described by

$$Re = \frac{\rho u d}{\mu},$$

where ρ and μ are the density and dynamic viscosity of kerosene, u is the bulk velocity of kerosene flow, d is the hydraulic diameter of the duct.

The Grashof number is described by

$$Gr = \frac{g\alpha_v \Delta T d^3}{\upsilon},$$

where g is gravitational acceleration, α_v and υ are volume expansion coefficient and kinematic viscosity of kerosene, ΔT is temperature difference between duct wall and kerosene bulk.

The heat transfer coefficient is described by

$$h = \frac{q_w}{T_w - T_f},$$

where q_w is wall heat flux, T_w and T_f are wall temperature and bulk temperature.

The Nusselt number is described by

$$Nu = \frac{hd}{k},$$

where h is the heat transfer coefficient, k is the thermal conductivity of kerosene. The average Nusselt number $\overline{Nu}$ is defined as the average value of the Nusselt number on the wall surface.

The total friction factor is described by

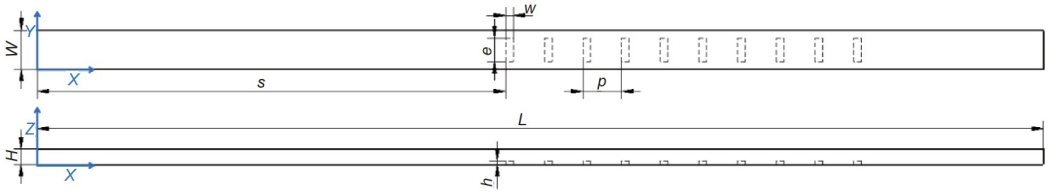

Figure 1 Schematic of geometrical configuration of the rectangular duct.

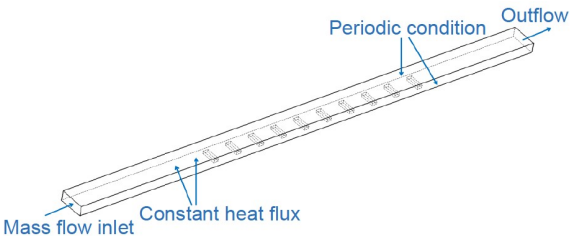

Figure 2 Schematic of boundary condition of the rectangular duct.

$$f = \frac{\Delta P d}{\frac{1}{2}\rho u^2 L},$$

where ΔP is the pressure loss from duct inlet to outlet, L is the duct length.

The skin friction coefficient is described by

$$c_f = \frac{\tau_w}{\frac{1}{2}\rho u^2},$$

where τ_w is wall shear stress.

The overall thermal performance factor (TP) is described by

$$TP = \frac{\overline{Nu}/\overline{Nu_0}}{(f/f_0)^{\frac{1}{3}}},$$

where $\overline{Nu_0}$ represent the average Nusselt number on the smooth wall and f_0 denotes the total friction factor of the smooth duct.

Table 1 summarizes the parameters of all cases involved in this paper. Kerosene flows in the small rectangular duct with the rectangular ribs of various heights from 0 to 1.5 mm are studied.

3. Numerical method and validation

3.1 Numerical validations

The incompressible steady-state Reynolds averaged Navier Stokes equations are taken as the governing equations and solved by the finite volume method in this current numerical study. The SIMPLEC algorithm is used to couple velocity and pressure. The results of the average Nusselt number and Nusselt number distribution are compared. Table 2 shows the comparison between the average Nusselt number obtained by numerical simulations of four different turbulence models and the experimental results of SriHarsha et al. [9] on air duct flow. The cross-section of the test duct used in Ref. [9] is 40 mm × 40 mm with arrays of rectangular ribs on the bottom wall. It is apparent in Table 2 that the average Nusselt number predicted by the RNG k-ε model is in best agreement with the experimental result of SriHarsha et al. [9] and the relative error is also within 0.3%. Figure 3 further presents the distribution of the local Nusselt number with a comparison to the computational result by Shukla and Dewan [22]. Obviously, the present data calculated by the RNG k-ε model are in accord with the previous results. Hence, the RNG k-ε turbulence model, including the enhanced wall treatment, is adopted in this paper.

Table 1 Flow and rib parameters

Wall heat flux q_w (kW/m^2)	Inlet mass flow rate $\dot{m}$ (g/s)	Inlet temperature T (K)	Inlet pressure P (MPa)	Rib height h (mm)
500	12	300	4	0
				0.25
				0.5
				0.75
				1.0
				1.25
				1.5

3.2 Grid independence

In order to guarantee the accuracy of the numerical results, the independence of the grid has been verified. In the near-wall region, in order to exactly capture the changes in heat transfer and flow properties, the girds are stretched and the first gird size from the ribbed wall is satisfied $\Delta y^+ \leq 1$, as shown in Fig. 4. The kerosene flow in a rectangular duct is calculated, in which the bottom wall is equipped with ribs with the height of 0.5 mm. The numerical results of four different gird sizes with total numbers of 1, 1.5, 2, and 2.5 million are compared. The number of grids in each co-

Table 2 Average Nusselt number predicted by different turbulence models and the experimental data

Model	$\overline{Nu}/\overline{Nu_0}$	$\overline{Nu}/\overline{Nu_0}$ (exp)	Relative error (%)
RNG k-ε	2.52	2.51	0.30
Standard k-ε	2.60		3.60
SST k-ω	2.63		4.65
Standard k-ω	2.54		1.06

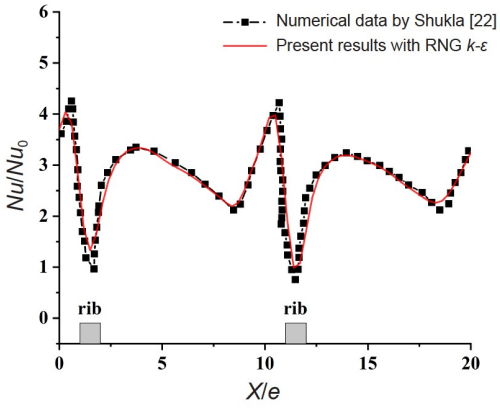

Figure 3 Local Nusselt number predicted by different turbulence models and the experimental data.

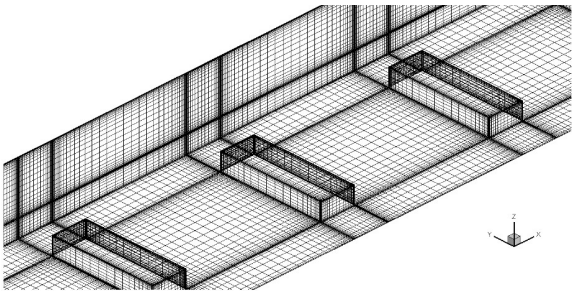

Figure 4 Grids near the rib wall.

ordinate direction is 600 × 45 × 45, 700 × 50 × 50, 800 × 55 × 55, and 850 × 60 × 60, respectively. Figure 5a and b shows the changes of average Nusselt numbers and total friction factors with the increase of the gird numbers. As shown in the figures, there is a significant difference between the results of 1 and 1.5 million grids. When the numbers of grids are greater than 1.5 million, the divergence reduces to less than 3%. Distributions of the Nusselt number along the duct centerline and the spanwise direction across the first duct center are respectively indicated in Fig. 6a and b. The centerline passes through the sixth rib along the streamwise direction (*X*-coordinate) and the spanwise direction (*Y*-coordinate), respectively. As shown in the figures, the Nusselt number does not change significantly anymore when the grids number reaches 2 million. Therefore, the total number of grids applied for this present simulation is 2 million.

4. Results and discussion

The rectangular duct with 0.5 mm height ribs is presented as the standard case. The results are compared with the smooth duct in order to evaluate the heat transfer enhancement of the ribbed duct, especially the increased ratios of the average Nusselt number and the total friction factor. Vortex structures of the flow field are then analyzed, and the mechanisms of the rib effects on the heat transfer performance are revealed. Finally, the results of heat transfer and flow field in different rib heights are shown respectively, and the corresponding height of rib changes from 0.25 to 1.5 mm. In addition, taking into account the heat transfer enhancement and the increase of wall friction, the overall thermal performance factors are obtained to compare the influence of rib heights.

4.1 Results of the standard case

The average Nusselt number on the bottom wall with and without ribs as well as the total friction factor are shown in Table 3. It is noteworthy that the average Nusselt number, non-dimensional heat transfer coefficient, is increased by

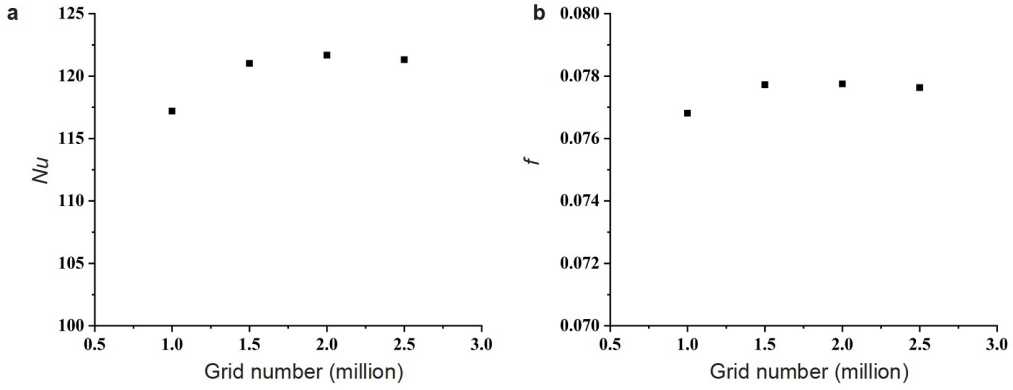

Figure 5 Results of Nusselt number and friction factor at different girds: **a** average Nusselt number, **b** total friction factor.

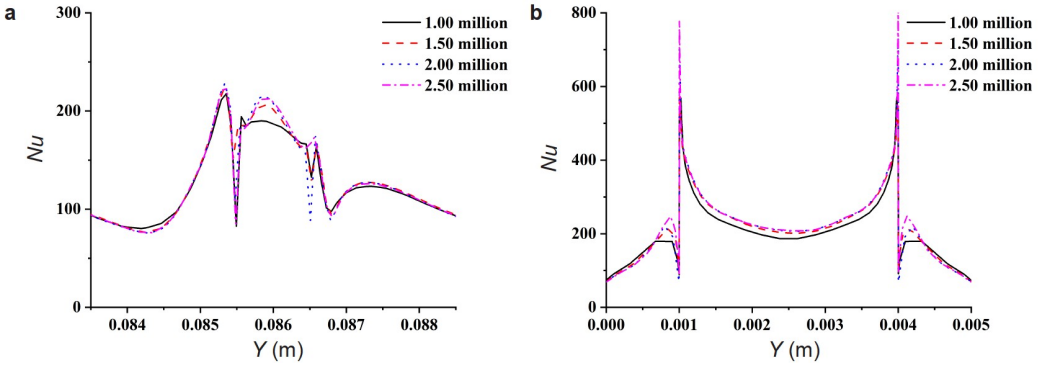

Figure 6 Nusselt number distribution along the duct centerline and the spanwise direction: **a** streamwise (*X*-coordinate), **b** spanwise (*Y*-coordinate).

Table 3 Average Nusselt number and total friction factor

Rib height h (mm)	Average Nusselt number $\overline{Nu}$	Total friction factor f
0	89.7	0.0250
0.5	121.61	0.0777
Increase ratio	35.57%	211%

35.57% with ribs. Furthermore, the total friction factor is also increased to 211% compared with that of the smooth wall.

Figure 7 presents the contour of the Nusselt number on the bottom wall with ribs. As shown in this figure, the Nusselt number distribution is approximately periodic with respect to ribs, and no apparent interaction between adjacent ribs is found. For each rib, the Nusselt number distribution is symmetric along the spanwise direction. There are two heat transfer enhancement zones around each rib, where the Nusselt number has the maximum value, and the details of their distributions are described in the following figure.

Figure 8a-c gives the three-dimensional distributions of the Nusselt number increase ratio around one of the ribs (the sixth rib) from three views in detail. The maximum values of the Nusselt number increase ratio appear at the front and the top side of each rib. These changes in the Nusselt number due to the rib effect are consistent with the experimental result of Wang and Sundén [23] for air channel flow.

Figure 9 presents the variation of the Nusselt number along the streamwise centerline (X-coordinate) of the fifth, sixth and seventh ribs. As shown in the figure, periodicity distribution is observed. There are two peaks of the Nusselt number increase ratio in front of and across the ribs, and their values are 1.5 and 1.45, respectively. Due to the local flow separation, a trough is found just behind the rib. The increased ratio of the average Nusselt number across a rib is positive with a value of about 0.5, indicating that the overall heat transfer on the wall with ribs is enhanced.

Figure 10 presents the variation of the Nusselt number along the spanwise centerline (Y-coordinate) across the sixth, eighth and tenth ribs. Distributions of the Nusselt number show symmetry with two peaks and two toughs near the side edges of the ribs. The Nusselt number peak and trough values indicate heat transfer enhancement and reduction, respectively. In a later section, the associated flow mechanisms will be described in detail. It is remarkable that the increase ratio of the average Nusselt number is prominent larger than zero and has a value of 1.5, indicating an overall heat transfer enhancement.

Figure 11a-c gives contours of iso-surface of Q quantity with a value of 10^5. Q is defined as $1/2 \times (\|\mathbf{\Omega}\|^2 - \|\mathbf{S}\|^2)$, where $\mathbf{\Omega}$ denote the vorticity tensor and $\mathbf{S}$ presents the shear strain tensor. The Q criterion defined by Hunt et al. [24] has been widely used to identify the vortex structure of the flow. The iso-surface with a sizeable positive value of Q means the region with strong vortices. As shown in Fig. 11a, three

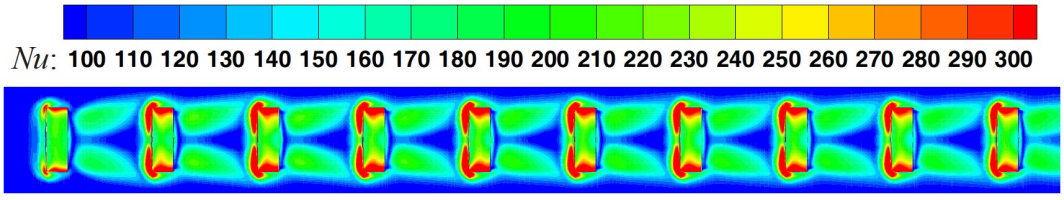

Figure 7 Contour of Nusselt number on the bottom wall with ribs.

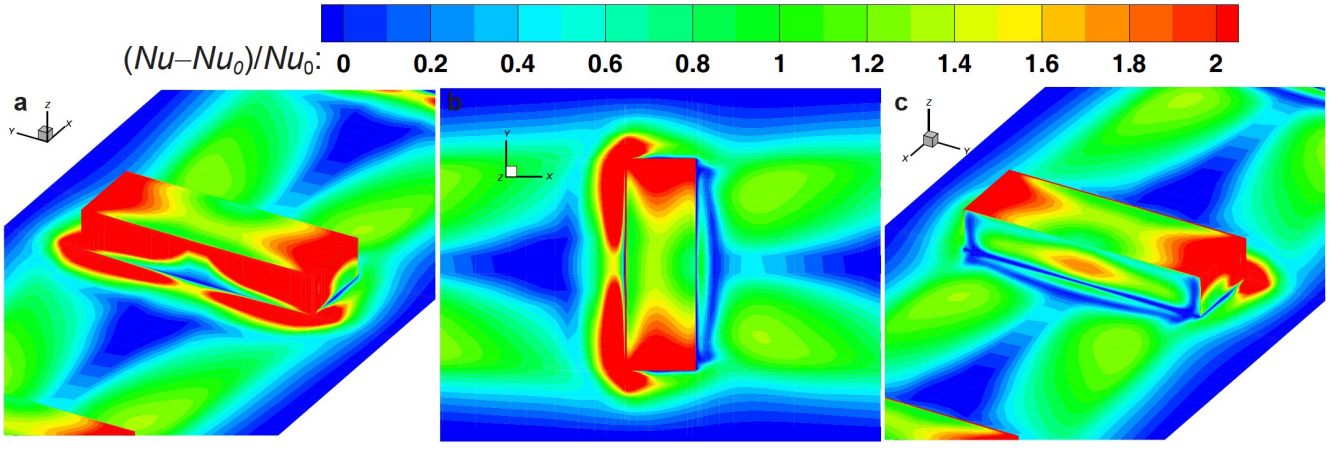

Figure 8 Three-dimensional distribution of Nusselt number increase ratio: **a** front view, **b** top view, **c** back view.

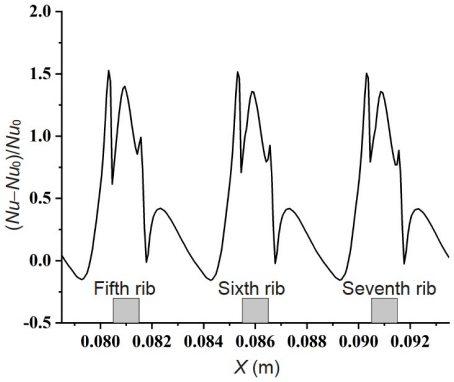

Figure 9 Variation of Nusselt number along the centerline in the streamwise direction (*X*-coordinate).

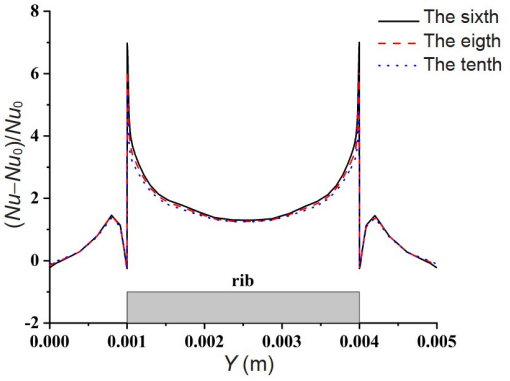

Figure 10 Variation of Nusselt number along the centerline in the spanwise direction (*Y*-coordinate).

dimensional vortices are generated around the ribs. The vortices show a periodic distribution in the streamwise direction as well as symmetry along the spanwise direction. Figure 11b and c gives details of the vortex around one of the ribs from the front and back views. It is found that the vortex is concentrated around ribs.

Figure 12a-c gives contours of the wall pressure and streamlines around the sixth rib. It seems clear that the existence of ribs induces flow rushing into the front of the rib, resulting in a high-pressure region. Therefore, the flow separates the upstream ribs as a result of the strong adverse pressure gradient. And the flow accelerates around the rib sides and leads to locally enhanced heat transfer. Then the sudden expansion of flow exists behind the rib. The kerosene rotates and forms large vortexes behind the rib and again reattaches at a further downstream location. The streamlines

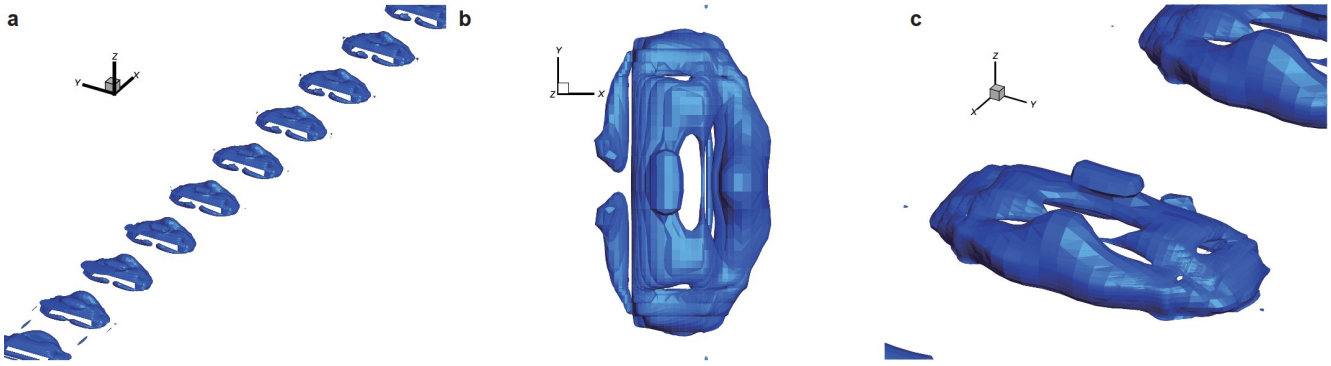

Figure 11 Vortical structure demonstrated by *Q* quantities: **a** whole view, **b** local contour of top view, **c** local contour of back view.

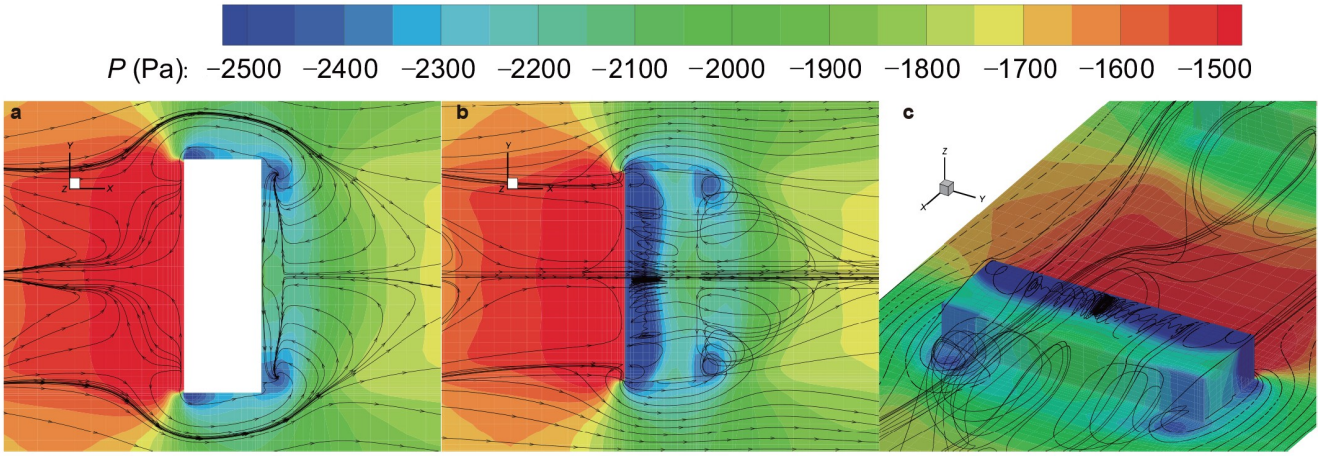

Figure 12 Contours of wall pressure and streamlines around the sixth rib: **a** surface streamlines of bottom, **b** volume streamlines of top view, **c** volume streamlines of back view.

around ribs have a similar structure to that of the experimental result reported by Liu et al. [25].

Figure 13a-c shows contours of the velocity magnitude and streamlines on different planes through the center point of the sixth rib. One can see that the vortex generated in the rib is complicated, and there are vortex components in all three directions. As shown in Fig. 13a, the spanwise feature of the vortex is the largest, resulting in strong mixing of the kerosene flow. From streamlines on the *y*-center plane, Fig. 13b, it is evident that the kerosene flowing through the rib structures forms four recirculations, which are located the upstream, top, behind, and downstream. In addition, the four recirculations around the rib structures have been marked by red bold outline in Fig. 13b. The vortex pattern is quite similar to that observed by Casarsa et al. [26] in experiments with the air flowing over the ribs.

According to Figs. 12 and 13, it is known that the rib structure makes the flow boundary layer separate, which enhances the disturbance of the main stream and strengthens the heat transfer. When kerosene flows through ribs, the cross-section decreases due to the existence of the rib, and the velocity magnitude increases greatly. Therefore, the acceleration of flow leads to the enhancement of local heat transfer in the front and on the side surface of the rib. At the same time, the separated flow is reattached with relatively high speed on the top surface of ribs, which also locally increases the heat transfer. In the rear of ribs, the kerosene flow suddenly expands and separates again, resulting in the formation of another larger-scale recirculation zone. Hence, local heat transfer is decreased just behind the ribs. The flow and vortex developments explain the formation of troughs and peaks of Nusselt number distribution, as described in Fig. 9.

4.2 Effect of rib height

Figure 14 presents the variation ratio of the average Nusselt number and total friction factor on the bottom wall with ribs of different heights. It is apparent that as the rib height increases, the variation ratio of the Nusselt number always increases. For the present study, when the rib height is 1.5 mm, the maximum heat transfer enhancement rate is 72.16% and the corresponding ratio of the rib-to-duct height is 0.75. Similarly, the friction factor variation ratio considerably increases with the rib height increasing, as shown in Fig. 14. The increase in friction factor indicates a more considerable cost of power input for cooling operation. Therefore, an appropriate cooling design should consider both heat transfer enhancement and wall friction augment. Here, the concept of thermal performance factor as defined in Section 2 is used to evaluate the overall performance of ribs, which can comprehensively consider both the enhanced heat transfer and the corresponding friction factor properties.

Figure 15 shows the changes in the overall thermal performance factor (*TP*) with ribs of different heights. As shown in this figure, the overall thermal performance factors decrease as the rib heights increase. Obviously, the cooling design requires higher operating input power costs so that the capacity of heat transfer can be enhanced to a greater extent. However, when the absolute value of the input power is not

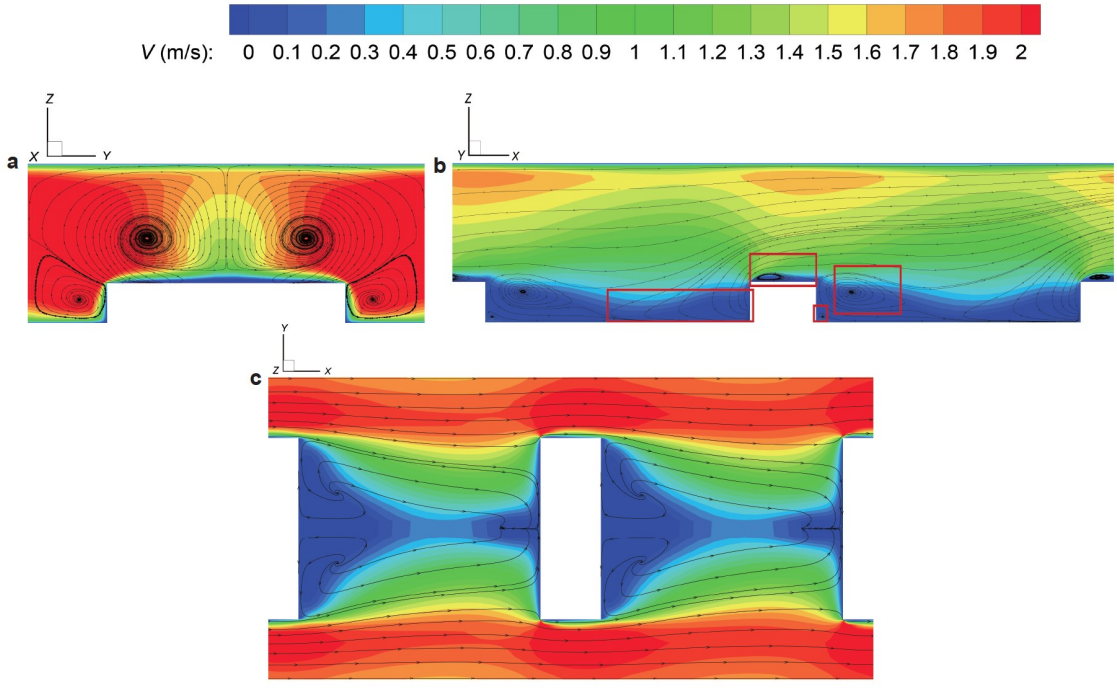

Figure 13 Contours of velocity magnitude and streamlines on different planes: **a** *x*-center plane, **b** *y*-center plane, **c** *z*-center plane.

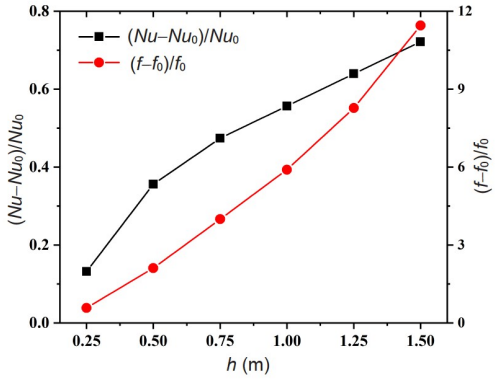

Figure 14 Variation of Nusselt number and friction factor increase ratio at different rib heights.

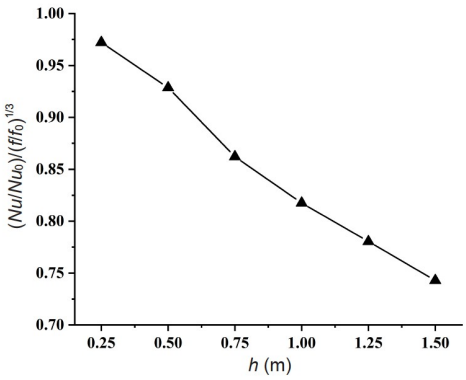

Figure 15 Variation of overall thermal performance factor at different rib heights.

enormous for the cooling design, the improvement of heat transfer is the most critical factor in many application cases.

Figure 16a-f gives contours of the Nusselt number on the bottom wall with ribs of different heights, where the height of ribs increases from 0.25 to 1.5 mm. As shown in these figures, when the height of ribs is not greater than 0.75 mm, the Nusselt number distribution around ribs shows periodicity and symmetry along the streamwise and spanwise direction. However, with the height of ribs increasing to 1.0 mm, the distribution of Nusselt number is not maintained periodically since the upstream ribs present larger Nusselt number distribution. It indicates that there are interactions between adjacent ribs when the rib is not less than 1.0 mm. The non-periodicity of Nusselt number distribution is also

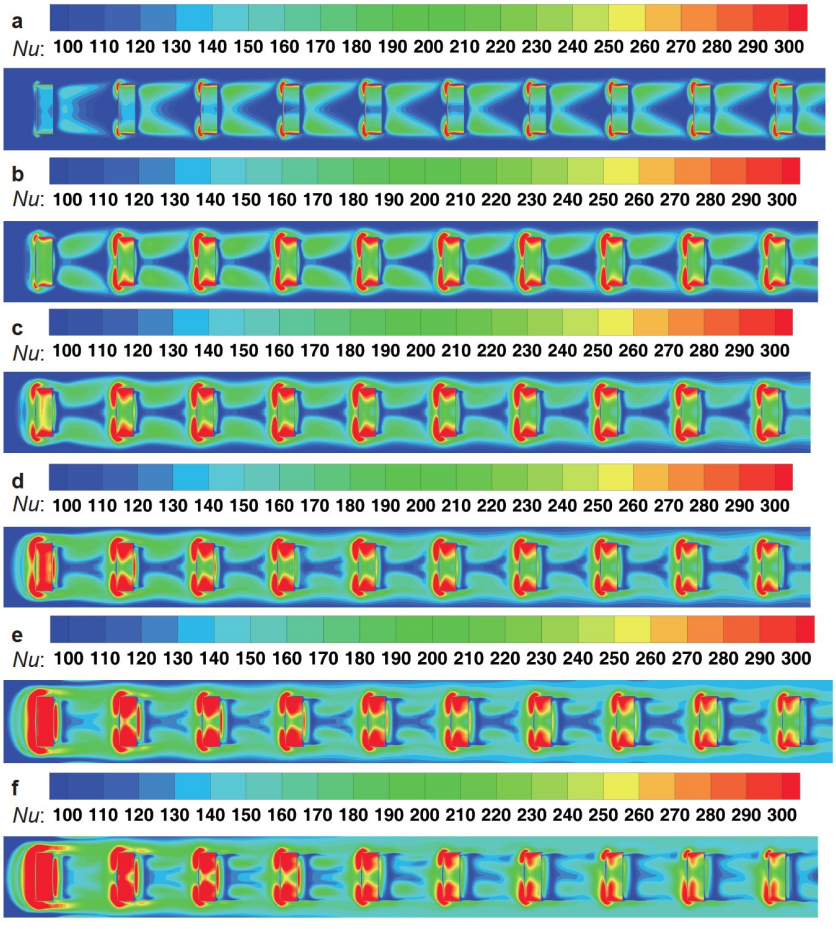

Figure 16 Contours of Nusselt number on the bottom wall at different rib heights: **a** 0.25 mm, **b** 0.5 mm, **c** 0.75 mm, **d** 1.0 mm, **e** 1.25 mm, **f** 1.5 mm.

observed by Liu et al. [25] and Xie et al. [27] in their numerical study of air rib flow. Nevertheless, the symmetry of the Nusselt number along the spanwise is generally kept for ribs with heights of 1.0 and 1.25 mm. As the height of ribs further increases to 1.5 mm, the Nusselt number distribution presents non-periodicity and asymmetry along the streamwise as well as the spanwise direction, respectively. In this case, a pronounced asymmetry of the Nusselt number distribution is found from the sixth rib along the spanwise direction. It indicates that for large rib height, the flow recirculation regions at the front corners of ribs are no longer symmetric, which is associated with unsteady properties of rib flow, as explained by Saha and Acharya [28] for a similar phenomenon. Another critical phenomenon, as shown in Fig. 16, is that when the height of ribs increases, areas with heat transfer enhancement at the front, top, and both sides of each rib become more prominent, which is considered to be the result of strong flow impingement in the front of ribs. Meanwhile, the regions of heat transfer reduction decrease since the flow accelerates with higher speed and quickly reattaches behind the ribs.

Figure 17a-f gives contours of the skin friction coefficient on the bottom wall with ribs of different heights. Compared with Fig. 16, the regions with larger and smaller surface skin friction coefficients basically correspond to the regions with enhanced and reduced heat transfer. Figures 16 and 17 show that there is a certain similarity between the heat transfer and flow friction which is termed as Reynolds analogy.

Figure 18a-f respectively shows contours of the wall pressure and surface streamlines on an *x*-*y* plane, which is 10^{-6} m above the bottom wall. When the height of ribs increases, the area with high pressure in front of the ribs becomes larger significantly and the pressure drop across the ribs also increases. The low-pressure region located downstream of the ribs also extends with increasing rib height. Correspondingly, streamlines around ribs present different vortical structures. The separation area induced by the adverse pressure gradient in front of the rib becomes more extensive as the height of ribs increases. The region of recirculation just located behind the ribs also extends. In summary, with the rise of rib height, the recirculation region and vortical structures become larger, leading to a more efficient heat transfer exchange between the coolant kerosene and the heated wall. Consequently, as the height of ribs increases, the convective heat transfer performance improves.

Figure 19a-f shows contours of velocity and distributions

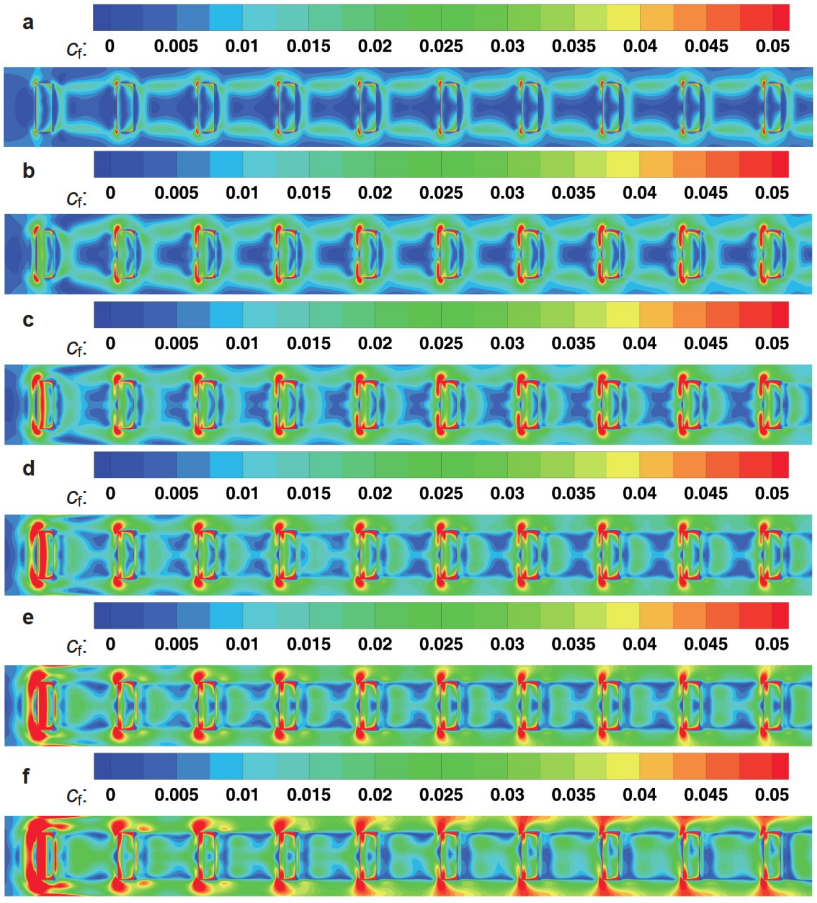

Figure 17 Contours of skin friction coefficient on the bottom wall at different rib heights: **a** 0.25 mm, **b** 0.5 mm, **c** 0.75 mm, **d** 1.0 mm, **e** 1.25 mm, **f** 1.5 mm.

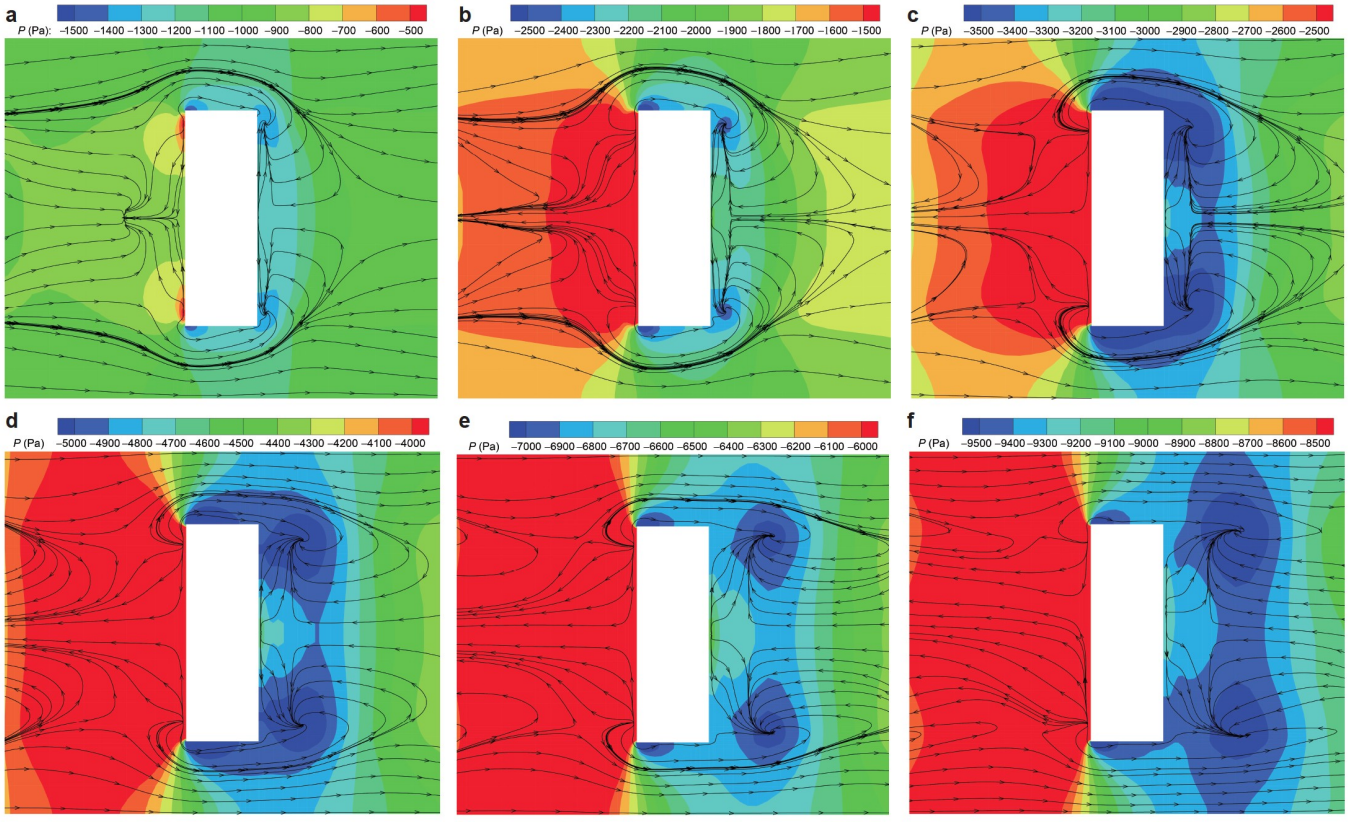

Figure 18 Contours of pressure and streamlines on an *x-y* plane at different rib heights: **a** 0.25 mm, **b** 0.5 mm, **c** 0.75 mm, **d** 1.0 mm, **e** 1.25 mm, **f** 1.5 mm.

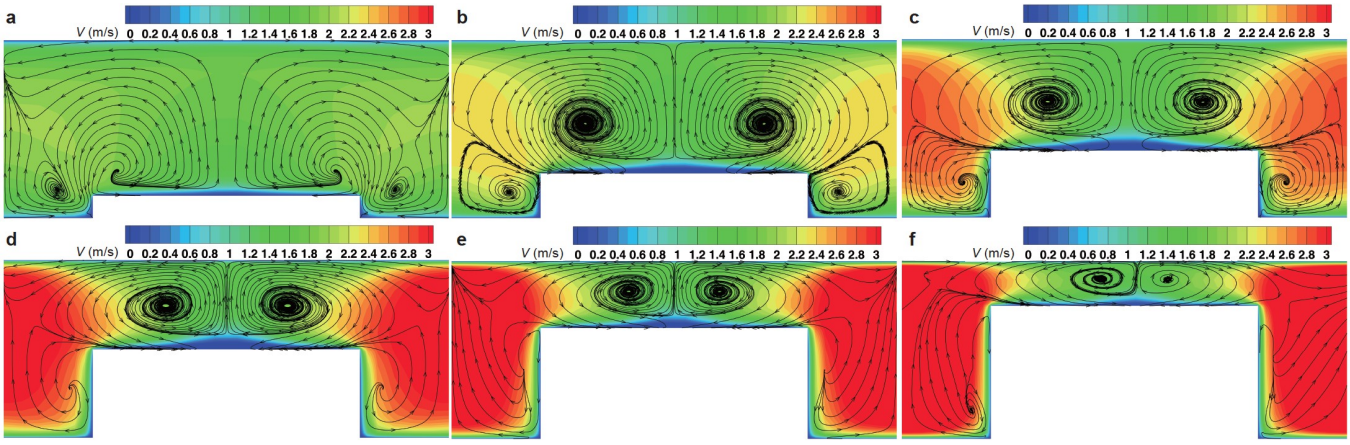

Figure 19 Contours of velocity and streamlines on a *y-z* plane at different rib heights: **a** 0.25 mm, **b** 0.5 mm, **c** 0.75 mm, **d** 1.0 mm, **e** 1.25 mm, **f** 1.5 mm.

of streamline on a *y-z* plane through the sixth rib center with different rib heights. As shown in the figures, symmetric vortices are formed above the rib top, and then the two vortices show a slight asymmetry as the rib height reaches 1.5 mm. The strong vortices and high-speed washing of coolant over the top surface result in enhanced local heat transfer. The streamwise vortices are generated on both sides of the rib, and the vortical strength first increases and then decreases as the height ribs increases. As a result of the reduced cross-section area, the enormous value of streamwise velocity is mainly located on both sides of the rib.

Figure 20a-f shows contours of turbulent kinetic energy and distributions of streamline on an *x-z* plane through the duct centerline with different rib heights. It seems clear that the spanwise vortex downstream of the rib becomes larger with a rise in rib height. As the rib height exceeds 0.75 mm, the vortex behind the rib is more significant and affects the flow around the next rib. The region with high turbulent kinetic energy is mainly located near the upstream and the top of ribs, corresponding to the peak values of Nusselt number as shown in Fig. 16. It is noteworthy that the region with high turbulent kinetic energy first enlarges with the

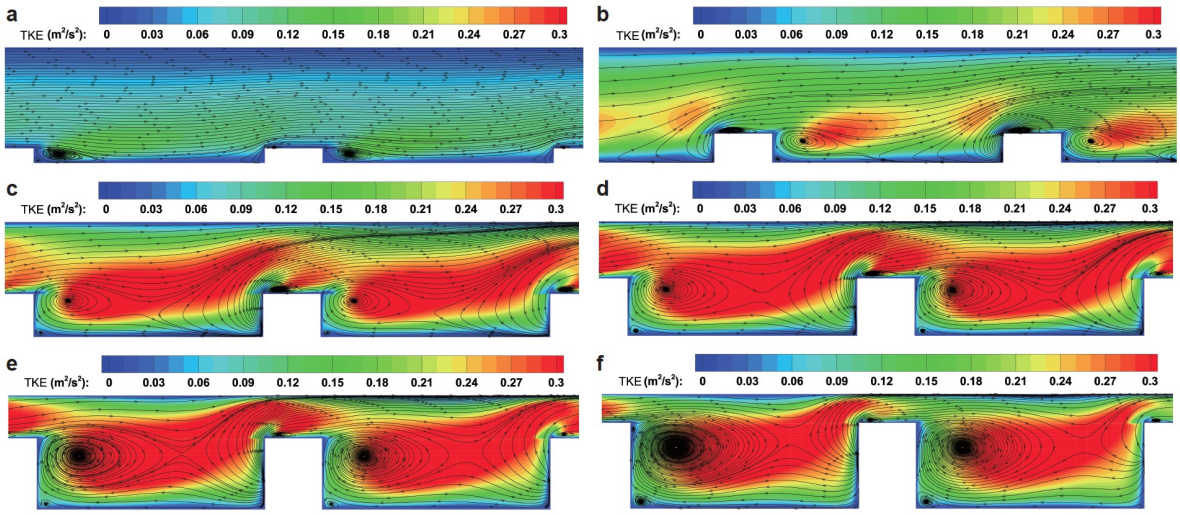

Figure 20 Contours of turbulent kinetic energy and streamlines on an *x*-*z* plane at different rib heights: **a** 0.25 mm, **b** 0.5 mm, **c** 0.75 mm, **d** 1.0 mm, **e** 1.25 mm, **f** 1.5 mm.

increase of the rib heights. When the height of the rib is greater than 1.0 mm, the high turbulent kinetic energy region gradually shrinks, indicating that the turbulence intensity is reduced. These are attributed to the fact that kerosene flow can not completely reattach before moving to the next rib, and the flow disturbance becomes smaller.

5. Conclusions

The heat transfer and flow field characteristics of kerosene in the cooling duct with a ribbed wall are well numerically studied by the ten components surrogate model of kerosene and the Reynolds average method combined with the RNG k-ε turbulence model. It is worth noting that the change of rib height will affect both the wall friction and convective heat transfer of the turbulent flow of kerosene. According to these current numerical results, the following conclusions may be obtained.

The existence of rib structures enhances the average Nusselt number, indicating that the overall heat transfer ability of kerosene has been improved. Because of the local flow acceleration and flow impingement, the peak values of the Nusselt number appear near the front, top, and both sides of the rib.

As the height of ribs increases, the average Nusselt number and total factor coefficient of the ribbed kerosene duct continue to increase. However, the overall thermal performance factor decreases when the height of ribs rises. When the height of ribs is 1.5 mm, the maximum heat transfer enhancement rate of kerosene flow is 72.16% and the ratio of the rib-to-duct height is 0.75 at the same time. In practical applications, the rib height can be designed as 0.5 mm and the ratio of rib-to-duct height is 0.25. The average Nusselt number is increased by 35.57% and the total friction factor is also increased by 211% compared to the values of a smooth wall.

The flow structures and corresponding vortices can perfectly explain the changes in Nusselt number and friction coefficient. When the ribs are short, the symmetric vortices are formed due to the pressure difference across ribs. As ribs become higher, the vortices become slightly asymmetric and lead to asymmetric distribution of the Nusselt number.

The regions with high turbulent kinetic energy are mainly located near the front and top surfaces of the rib, which brings about the locally enhanced heat transfer. When the height of ribs increases, the region with high kinetic energy first extends and then shrinks since the flow interaction between two adjacent ribs becomes more obvious as the rib height is larger than 1.0 mm.

This work is supported by the National Natural Science Foundation of China (Grant Nos. 12072351 and 11872367).

1 P. M. Ligrani, T. Blaskovich, and M. M. Oliveira, Comparison of heat transfer augmentation techniques, AIAA J. **41**, 337 (2003).
2 L. Wang, M. Salewski, and B. Sundén, Turbulent flow in a ribbed channel: Flow structures in the vicinity of a rib, Exp. Thermal Fluid Sci. **34**, 165 (2010).
3 Y. Rao, Z. Guo, and D. Wang, Experimental and numerical study of heat transfer and turbulent flow characteristics in three-short-pass serpentine cooling channels with miniature W-ribs, J. Heat Transfer **142**, 121901 (2020).
4 V. B. Gawande, A. S. Dhoble, and D. B. Zodpe, Effect of roughness geometries on heat transfer enhancement in solar thermal systems—A review, Renew. Sustain. Energy Rev. **32**, 347 (2014).
5 K. Sreekesh, D. K. Tafti, and S. Vengadesan, Large-eddy simulation investigation of modified rib shapes on heat transfer in a ribbed duct, J. Heat Transfer **143**, 112101 (2021).
6 G. Xie, J. Liu, P. M. Ligrani, and B. Sunden, Flow structure and heat transfer in a square passage with offset mid-truncated ribs, Int. J. Heat Mass Transfer **71**, 44 (2014).

7 R. Kamali, and A. R. Binesh, The importance of rib shape effects on the local heat transfer and flow friction characteristics of square ducts with ribbed internal surfaces, Int. Commun. Heat Mass Transfer **35**, 1032 (2008).

8 P. Promvonge, and C. Thianpong, Thermal performance assessment of turbulent channel flows over different shaped ribs, Int. Commun. Heat Mass Transfer **35**, 1327 (2008).

9 V. SriHarsha, S. V. Prabhu, and R. P. Vedula, Influence of rib height on the local heat transfer distribution and pressure drop in a square channel with 90° continuous and 60° V-broken ribs, Appl. Thermal Eng. **29**, 2444 (2009).

10 K. M. Kim, H. Lee, B. S. Kim, S. Shin, D. H. Lee, and H. H. Cho, Optimal design of angled rib turbulators in a cooling channel, Heat Mass Transfer **45**, 1617 (2009).

11 S. Skullong, C. Thianpong, and P. Promvonge, Effects of rib size and arrangement on forced convective heat transfer in a solar air heater channel, Heat Mass Transfer **51**, 1475 (2015).

12 N. Sharma, A. Tariq, and M. Mishra, Detailed heat transfer and fluid flow investigation in a rectangular duct with truncated prismatic ribs, Exp. Thermal Fluid Sci. **96**, 383 (2018).

13 S. Oleiwi, and R. Al-Turaihi, The effect of ribs height in two phase flow (air-water) on heat transfer coefficient in vertical ribbed duct, Ain Shams Eng. J. **10**, 801 (2019).

14 K. Xu, L. Tang, and H. Meng, Numerical study of supercritical-pressure fluid flows and heat transfer of methane in ribbed cooling tubes, Int. J. Heat Mass Transfer **84**, 346 (2015).

15 X. Li, J. Qin, S. Zhang, N. Cui, and W. Bao, Effects of microribs on the thermal behavior of transcritical n-Decane in asymmetric heated rectangular mini-channels under near critical pressure, J. Heat Transfer **140**, 122402 (2018).

16 D. R. Sobel, and L. J. Spadaccini, Hydrocarbon fuel cooling technologies for advanced propulsion, J. Eng. Gas Turbines Power **119**, 344 (1997).

17 H. Huang, L. J. Spadaccini, and D. R. Sobel, Fuel-cooled thermal management for advanced aeroengines, J. Eng. Gas Turbines Power **126**, 284 (2002).

18 W. Fan, and F. Zhong, Numerical study of turbulent convective heat transfer of aviation kerosene in coiled pipes, J. Heat Transfer **143**, 061801 (2021).

19 G. Dang, F. Zhong, Y. Zhang, and X. Zhang, Numerical study of heat transfer deterioration of turbulent supercritical kerosene flow in heated circular tube, Int. J. Heat Mass Transfer **85**, 1003 (2015).

20 F. Zhong, X. Fan, G. Yu, J. Li, and C. J. Sung, Heat transfer of aviation kerosene at supercritical conditions, J. Thermophys. Heat Transfer **23**, 543 (2009).

21 Z. Tao, Z. Cheng, J. Zhu, and H. Li, Effect of turbulence models on predicting convective heat transfer to hydrocarbon fuel at supercritical pressure, Chin. J. Aeronaut. **29**, 1247 (2016).

22 A. K. Shukla, and A. Dewan, Computational study on effects of rib height and thickness on heat transfer enhancement in a rib roughened square channel, Sādhanā **41**, 667 (2016).

23 L. Wang, and B. Sundén, Experimental investigation of local heat transfer in a square duct with continuous and truncated ribs, Exp. Heat Transfer **18**, 179 (2015).

24 J. C. Hunt, A. A. Wray, and P. Moin, in Eddies, streams, and convergence zones in turbulent flows: Studying Turbulence Using Numerical Simulation Databases, 2. Proceedings of the 1988 Summer Program (NASA, 1988).

25 J. Liu, J. Wang, S. Hussain, L. Wang, G. Xie, and B. Sundén, Application of fractal theory in the arrangement of truncated ribs in a rectangular cooling channel (4:1) of a turbine blade, Appl. Thermal Eng. **139**, 488 (2018).

26 L. Casarsa, M. Cakan, and T. Arts, in Characterization of the velocity and heat transfer fields in an internal cooling channel with high blockage ratio: ASME Turbo Expo 2002: Power for Land, Sea, and Air (Amsterdam, 2022).

27 G. Xie, J. Liu, W. Zhang, G. Lorenzini, and C. Biserni, Numerical prediction of turbulent flow and heat transfer enhancement in a square passage with various truncated ribs on one wall, J. Heat Transfer **136**, 011902 (2014).

28 A. K. Saha, and S. Acharya, Unsteady RANS simulation of turbulent flow and heat transfer in ribbed coolant passages of different aspect ratios, Int. J. Heat Mass Transfer **48**, 4704 (2005).

微肋高度对矩形通道内煤油流动与传热性能的影响研究

李冼, 仲峰泉, 邢云绯

摘要 本文针对航空煤油数值研究微肋高度和物性变化对矩形通道内湍流流动及对流换热的耦合影响. 采用雷诺平均方法并结合RNG k-ε湍流模型以及煤油的十组分替代模型进行流动与传热计算, 从而获得了不同高度的矩形微肋的流场演变和传热特性. 结果表明, 煤油流经微肋结构产生三维旋涡结构, 进而显著影响局部流动, 导致不同位置处的对流换热性能增强或者减弱. 此外, 研究发现, 随着微肋高度的增加, 带有微肋结构底面的平均努塞尔数和壁面摩擦系数也随之增加. 在本研究中, 当微肋与管道高度之比为0.75时, 最大的强化传热效率为72.16%.